Voltage and frequency control of microgrid in presence of micro-turbine interfaced to matrix converter

Mahdi Toupchi Khosroshahi[1], Ali Ajami[1], Tole Sutikno[2,3]
[1]Department of Electrical Engineering, Azarbaijan Shahid Madani University, Tabriz, Iran
[2]Master Program of Electrical Engineering, Faculty of Industrial Technology, Universitas Ahmad Dahlan, Yogyakarta, Indonesia
[3]Embedded System and Power Electronics Research Group, Yogyakarta, Indonesia

ABSTRACT

The active and reactive load changes have a significant impact on voltage and frequency. In this paper, in order to stabilize the microgrid (MG) against load variations in islanding mode, the active and reactive power of all distributed generators (DGs), including energy storage (battery), diesel generator, and micro-turbine, are controlled. The micro-turbine generator is connected to MG through a three-phase to three-phase matrix converter, and the droop control method is applied for controlling the voltage and frequency of MG. In addition, a method is introduced for voltage and frequency control of micro-turbines in the transition state from grid-connected mode to islanding mode. A novel switching strategy of the matrix converter is used for converting the high-frequency output voltage of the micro-turbine to the grid-side frequency of the utility system. Moreover, using the switching strategy, the low-order harmonics in the output current and voltage are not produced, and consequently, the size of the output filter would be reduced. In fact, the suggested control strategy is load-independent and has no frequency conversion restrictions. The proposed approach for voltage and frequency regulation demonstrates exceptional performance and favorable response across various load alteration scenarios. The suggested strategy is examined in several scenarios in the MG test systems, and the simulation results are addressed.

Corresponding Author:

Ali Ajami
Department of Electrical Engineering, Azarbaijan Shahid Madani University
Tabriz, Iran
Email: ajami@azruniv.ac.ir

1. INTRODUCTION

The current surge in electricity consumption is causing frequent power outages due to strains on transmission and generation infrastructure. The efficiency of central plants is restricted to a maximum of 35% due to transmission and generation losses. The rise in greenhouse gas emissions can be ascribed to the inefficiency of the electrical system. This resulted in extensive research to fulfill rising energy demand without compromising the transmission system's capacity. A feasible solution is to use distributed generation (micro-turbines, photovoltaic (PV) arrays, wind turbines, and so forth) in the distribution system. However, if these new dispersed generation technologies are implemented without a plan, they will cause further challenges. As a result, microgrids were proposed as a novel network architecture for distribution systems. All distributed generators (DGs) in an autonomous microgrid should be able to control the system's voltage and frequency while sharing active and reactive power. It is critical to establish effective load sharing by the DGs when contemplating the interfacing of a microgrid with the utility system. One of the most desirable

features of microgrids (MGs) is load sharing without communication between converters, as the grid can be sophisticated and stretch across a vast geographic area. The frequency droop characteristic is a common strategy used to achieve this goal, allowing for local control of parallel converters to supply the system with the desired real and reactive power levels. The frequency and magnitude of the fundamental voltage are frequently used to control the distribution of actual and reactive power [1], [2]. The effects of such load sharing on system stability have been investigated in [3]–[6]. On the one hand, low inertia is a big issue with microgrids. That is, microgrids are unstable when disturbed or faulty. The microgrid, on the other hand, will respond to load changes or islanding mode more slowly as the number of DGs grows, due to its increased mass. [7] discusses the transient stability of a converter-based microgrid (with a converter connected).

The study conducted in [6] examines the analysis and modeling of the autonomous operation of a power system based on converters and distributed generation. The converters are managed using a voltage and frequency droop technique. Each sub-module of the system has been assigned a state-space model, and all the modules are then merged onto a shared reference frame. The model encompasses the intricacies of the control loops employed by the converter but excluding the switching operation. Normal proportional integral (PI) controllers are utilized to regulate voltage and current. The original design of micro turbines for electricity generation has been considered to cater to isolated loads that are not accessible through the distribution network of any utility [3]. The functioning of micro-turbines at high speeds and frequencies, specifically 96,000 rpm and 1,600 Hz, necessitates the utilization of power electronics to achieve an output voltage of 480/220 V at 50/60 Hz. In this study, a novel direct alternating current to alternating current (AC-AC) converter is proposed as a means to establish a connection between a high-speed micro-turbine generator (MTG) and the utility grid. The matrix converter (MC) is a converter architecture that enables direct conversion of AC to AC via a matrix.

The principles of operation have been covered in studies [8] and [9]. Analyzed in [10]–[18] are control strategies and/or switching approaches. Space vector modulation (SVM) is predominantly employed in both direct and indirect multicarrier networks (MCs). The main limitations of SVM include heightened levels of harmonic distortion in the output waveforms, a diminished voltage transfer ratio, and limited manipulability of the input power factor. One drawback of SVM is its high implementation costs, especially in terms of training data and feature space dimension. The study [17] employs a wind turbine that is connected to a three-phase matrix converter and utilizes SVM modulation for control. This paper asserts a reduction in overall harmonic distortion in the output voltage, however, there is a lack of experimental evidence to substantiate this assertion. However, it is evident that one of the primary drawbacks of the SVM approach is the presence of significant overall harmonic distortion in the output waveforms. The technique of directly modulating the space vector, as described in study [18], aims to enhance the quality of matrix converters by generating input and output currents in sine form. However, there is currently no evidence to support the improvement in voltage transfer ratio. Pulse width modulation (PWM) approaches in power electronics systems offer significant advantages, such as the reduction of harmonic distortion and noise in the output waveform. This leads to improved power quality and a decrease in electromagnetic interference (EMI). Additionally, the converter's efficiency and dependability are enhanced. Furthermore, PWM streamlines the process of designing and implementing the converter by eliminating the need for intricate filters, transformers, or feedback circuits.

The implementation of control techniques and switching methods in grid linked modes is limited, and their utilization in microgrids with diverse energy sources and load fluctuations is also lacking. In study [19], despite the implementation of a novel modulation scheme capable of maintaining a nearly constant duty cycle of gate signals irrespective of variations in output voltage, there is a lack of empirical evidence to assess the impact of load fluctuations. Furthermore, the total harmonic distortion (THD) of the output voltage without a filter is significantly noticeable, necessitating the usage of filters with bigger components. The topic of commutation strategies is addressed in research studies [20]–[22]. The evaluation and study of MC performance can be found in research studies [23]–[28], and the applications of MC have been extensively addressed in research studies [28], [29]. The elimination of the direct current (DC)-link capacitor, which is an integral component of an AC-DC-AC converter system, is achieved through the direct AC-AC conversion facilitated by the MC. The primary benefit of MCs is as follows. The study [30] presents a variety of converter topologies, comparing and evaluating them in terms of their ability to manage input power factor, output voltage and phase, and component count. When examining the qualities of each converter design, we explore alternative applications for commonly used converters with DC-link energy storage devices. This paper's primary contributions, in comparison to other converters lacking a DC-link energy storage component, are the enhancement of input current quality and the reliability of the converter. Input and output power quality can be improved by utilizing these converters. The lack of the electrolytic capacitor as a DC-link energy storage component enhances the longevity of power converters, hence improving their reliability. To clarify, the inclusion of a DC capacitor results in an increase in the converter's volume, size, and footprint, while simultaneously decreasing the dependability and mean-time-before-failure (MTBF) of the entire system.

One of the challenges encountered in AC-AC conversion arises when there is a substantial imbalance in the input voltages. In this particular scenario, the majority of control approaches are unable to generate the intended output voltage. The primary topic of the research study [31] is the examination of the modeling, control, and stability analysis of a quasi-Z-source matrix converter (qZSMC) which serves as the grid interface of a permanent magnet synchronous generator-based wind energy conversion system (PMSG-WECS). This research focuses on the analysis of a single energy source (PMSG-WECS) connected to a qZSMC at various wind speeds (input). However, the results obtained from this analysis have not been compared across different load variations. Furthermore, the simulation is limited to grid-connected mode and does not include the results for islanding mode operation. Hence, the proposed control technique ensures the attainment of the intended output voltage, even in the presence of imbalanced input voltages and varying load fluctuations across three energy sources. The control mechanism being presented exhibits independence from the load and does not impose any limitations on frequency conversion. This contributes to the stability of micro-turbines and other distributed generators, even while connected to the grid in islanding mode, even when the load conditions change. Furthermore, the use of the suggested control method effectively mitigates the generation of low-order harmonics in both the input and output values. This results in a reduction in the size of the necessary filters. Moreover, it offers a superior output/input voltage transfer ratio compared to traditional approaches and the approach suggested in [18]. Another concern in DGs of a microgrid is that any alteration in the frequency and voltage of other DGs has an impact on the output voltage MTG. The solution presented in this paper effectively addresses this issue. Frequency and voltage oscillations in microgrids are commonly attributed to load fluctuations, particularly when the microgrid is isolated from the utility grid, a phenomenon known as islanding mode.

2.   MICROGRID SYSTEM CONFIGURATIONS AND FEATURES

The microgrid has the capability to function as either a DC grid, AC grid, or high frequency AC grid. AC microgrids can exist in either a single-phase or three-phase configuration. It has the capability to be linked to power distribution networks of either low voltage or medium voltage. This study examines microgrids that are integrated into the utility power grid's distribution system and function as a component of the distribution system. Figure 1 depicts a visual representation of a microgrid configuration, whereby multiple DG components, such as an energy storage (battery), diesel generator, and micro-turbine system, are interconnected with the distribution feeders. At the point of common coupling (PCC), the microgrid is linked to the mains grid via a separation mechanism, typically a static transfer switch (STS). This device facilitates the rapid disengagement of the microgrid from the utility in the event of a utility fault. In essence, a microgrid can be conceptualized as a utility distribution system comprising power generators and control devices.
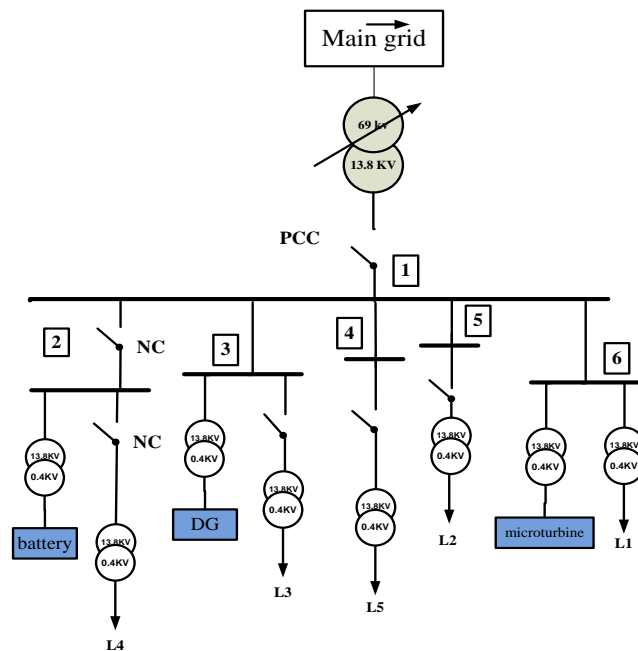
Figure 1. The 6-bus test system

A microgrid can be operated in two distinct modes: grid-connected mode and islanding mode. The primary purpose of the DG units, when linked to the utility grid, is to produce electricity and offer localized voltage and power assistance. The DG units can generate regulated reactive power through the use of connecting power converters. Consequently, the reduction of line loss can lead to a significant enhancement in the overall efficiency of the system. The purposeful islanding mode is an alternative operational mode. This occurrence arises when the microgrid is isolated from the primary grid. In order to ensure a dependable islanding operation, it is necessary to properly regulate the DGs to satisfy the following three criteria. Initially, the combined power production from all the DGs in the microgrid must align with the load demand. Consequently, precise load distribution among the DG units would take place, such as in the event of a power outage in the primary grid, and remains operational to supply electricity to nearby loads. Additionally, it is crucial to observe the power capacity of each DG in order to prevent potential harm to any DG. Additionally, the DGs are responsible for regulating voltage levels to ensure that all feeder voltages remain within their designated ranges. Additionally, it is necessary for all DGs to be synchronized with one another and offer microgrid frequency control. The importance of a rapid and reliable islanding detection technique for each DG unit in order to ensure the correct operation of a microgrid is attributed to the distinct control objectives of the two operation modes.

3. INTERFACING POWER ELECTRONICS AND ITS MODULATION STRATEGY

Instead of utilizing a rectifier and an inverter, one might employ a cycloconverter or a MC to establish a connection between the micro-turbine generator and the grid. The converters depicted in Figure 2 are designed to directly transform AC voltages at one frequency into AC voltages at another frequency, while providing the ability to adjust the magnitude. The drawbacks of these converters lie in their lack of a DC or AC connection for energy storage. The absence of energy storage within the converter results in a direct impact of any fluctuations occurring on either side of the converter on the other side. Furthermore, unlike the dc link converter or the flying capacitor converter (FCC), it is not feasible to establish a connection between these converters and a battery or any other power source. The utilization of a cycloconverter remains viable for micro-turbines operating within the high frequency range. A cycloconverter may immediately convert the three-phase AC voltage to three-phase high frequency AC voltage, eliminating the need to convert the generator power to DC and subsequently to high frequency AC.
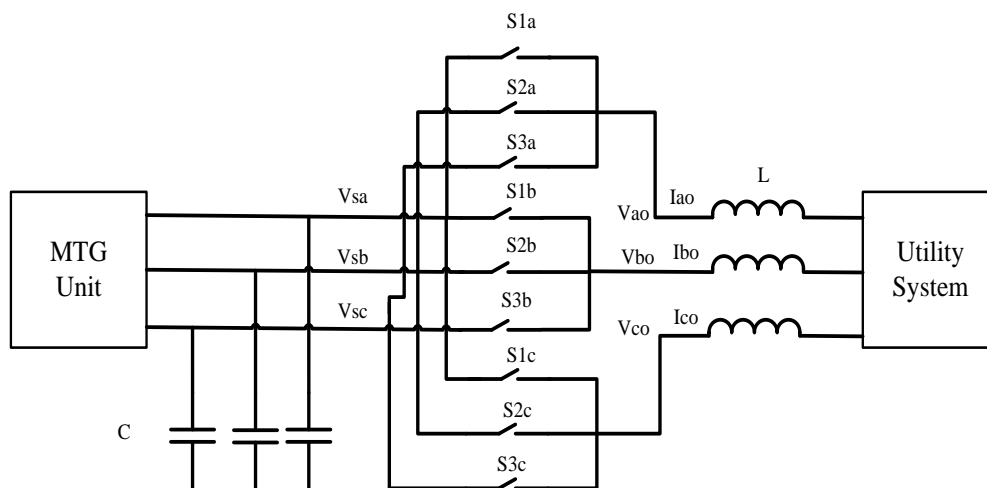

Figure 2. The MTG connect to the utility grid through MC

The PWM approach is a frequently employed control method for regulating the waveform of the output voltage. This technique involves modifying the duty cycle of switches at high switching frequencies in order to get the desired output voltage and current at low frequencies. Put simply, the PWM technology has the capability to regulate the output voltage by effectively switching between the permissible states. This ensures that the average value of the output voltage aligns with the intended waveform. By employing the technique described in study [16], the intended sinusoidal voltage is produced by sampling segments of the input waveforms.

This section presents an exposition of the research findings, accompanied by a thorough analysis and exhaustive examination. The findings can be visually represented through figures, graphs, tables, and other visual aids, facilitating the reader's comprehension [14], [15]. The conversation can be divided into multiple sub-sections.

3.1. The MC switching strategy

In the modulation approach being presented, it is assumed that the switching frequency in each area is $f_s = \frac{1}{T_s}$. Throughout the jth sample period ($T_s^j; j = 1,2,3,\dots$), each sampling period is partitioned into two-time intervals, which are as (1).

$$T_s^{\,j} = t_{\max}^{\,j} + t_{\min}^{\,j})$$

(1)

Throughout the specified time interval, the highest input voltage will be transmitted to the output, while the lowest input voltage will be transmitted to the output. This sequential procedure will continue for the remaining sample periods. Based on the data shown in Table 1, the general relationships between and for both converters described can be characterized as (2) and (3).

$$v_{\max}(t) = V_{\max} \sin(w_i t + \varphi_{\max})$$

(2)

$$v_{\min}(t) = V_{\max} \sin(w_i t + \varphi_{\min})$$

(3)

Table 1. Permitted modes for MC with six switches

Mode	On switches	V_o
1	$S_{1a} \& S_{2b}$	$v_{sa} - v_{sb}$
2	$S_{1a} \& S_{3c}$	$v_{sa} - v_{sc}$
3	$S_{2b} \& S_{3c}$	$v_{sb} - v_{sc}$
4	$S_{1b} \& S_{2a}$	$v_{sb} - v_{sa}$
5	$S_{3a} \& S_{1c}$	$v_{sc} - v_{sa}$
6	$S_{2c} \& S_{3b}$	$v_{sc} - v_{sb}$

3.2. Algorithms

In order to ensure that the fundamental component of the generated output voltage aligns with the waveform of the intended output voltage, it is necessary to carefully select the time intervals of and during the sampling period. The average output voltage can be expressed as follows, assuming a high switching frequency ($fs \gg fi$ and $fs \gg fo$).

$$v_o(t) = \frac{1}{T_s}\left[t_{\max}^{\,j} v_{\max}(t) + t_{\min}^{\,j} v_{\min}(t)\right]$$

(4)

Equation (4) can be reformulated in the following manner:

$$v_o(t) = \sum M_K(t) . v_k(t) \text{ for } k = max, min$$

(5)

The modulation function, denoted as $M_K(t)$, is defined in (5) as (6):

$$M_K(t) = \frac{t_k}{T_s} \text{for } k = max, min$$

(6)

The modulation function must always be in accordance with (7):

$$\sum_k M_K(t) = 1 \text{for } k = max, min \ 0 \leq M_K(t) \leq 1$$

(7)

Equation (4) demonstrates that the desired output voltage can be generated by combining v_{max} and v_{min} during time intervals t_{max}^j and t_{min}^j. The time periods t_{max}^j and t_{min}^j are computed by considering (1), (2), and (3).

$$t_{max} = T_s \frac{q \sin(w_o t) - x \sin(w_i t + \varphi_{min})}{x \sin(w_i t + \varphi_{max}) - x \sin(w_i t + \varphi_{min})} \tag{8}$$

$$t_{min} = T_s - t_{max} \tag{9}$$

Which x represents the correlation between v_{max} and v_{min}. The expression is as (10), (11):

$$x = \frac{v_{max}}{v_{im}} \tag{10}$$

$$q = \frac{v_{om}}{v_{im}} \tag{11}$$

Figure 3 presents a comprehensive flowchart illustrating the logical process employed for the conversion of three-phase to three-phase MC. The values of v_{max} and v_{min} are derived based on the information provided in Table 1. The values of the t_{max}^j and t_{min}^j are computed for each sample period in a manner that ensures the fundamental component of the generated output voltage aligns with the desired output voltage. It is crucial to acknowledge that the values of t_{max}^j and t_{min}^j are calculated in a manner that ensures the average output voltage per modulation cycle aligns with the desired output voltage. After careful consideration of (8), it becomes evident that the proposed approach is not influenced by the load. Furthermore, it is possible to generate the desired output voltage even when the input voltages are unbalanced. In the jth sample period, it is necessary to modify (1) and the subsequent relationships in order to determine the values of t_{max}^j and t_{min}^j.

$$\begin{aligned} 0 \le t_{max}^j \le T_s^j \\ 0 \le t_{min}^j \le T_s^j \end{aligned} \qquad for \quad j = 1, 2, 3, ..., \tag{12}$$
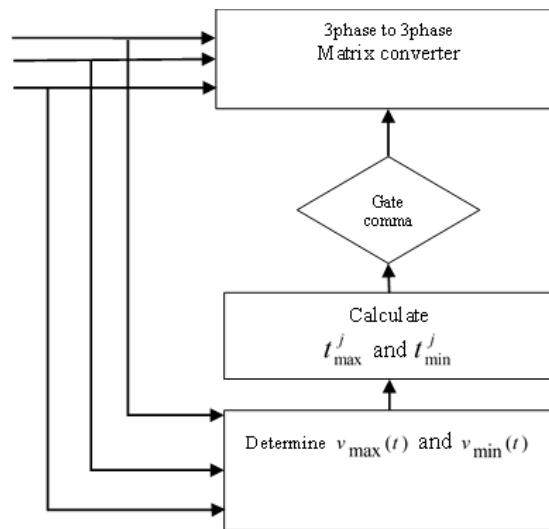

Figure 3. The MTG connect to the utility grid through MC

3.3. Droop control-based voltage and frequency control

The simplified block diagram of a micro-grid-connected microgrid is depicted in Figure 4. The power circuit consists of a three-leg MC with an LC filter and a coupling inductor, while the control structure is composed of three control loops. In order to generate the magnitude and frequency of the fundamental output voltage of the MC based on the droop characteristics, a power-sharing controller is employed. This controller emulates the operation of a conventional synchronous generator. Additionally, a voltage controller is utilized to synthesize the reference filter-inductor current vector. Furthermore, a current controller is employed to generate the command voltage vector that will be synthesized by a PWM module. It is

imperative that both the voltage and current control loops exhibit sufficient damping capabilities to effectively mitigate the effects of the output T-filter, which consists of the LC filter and the coupling inductor. The output impedance of the MC is influenced by the coupling inductor in order to minimize the active-reactive power coupling.
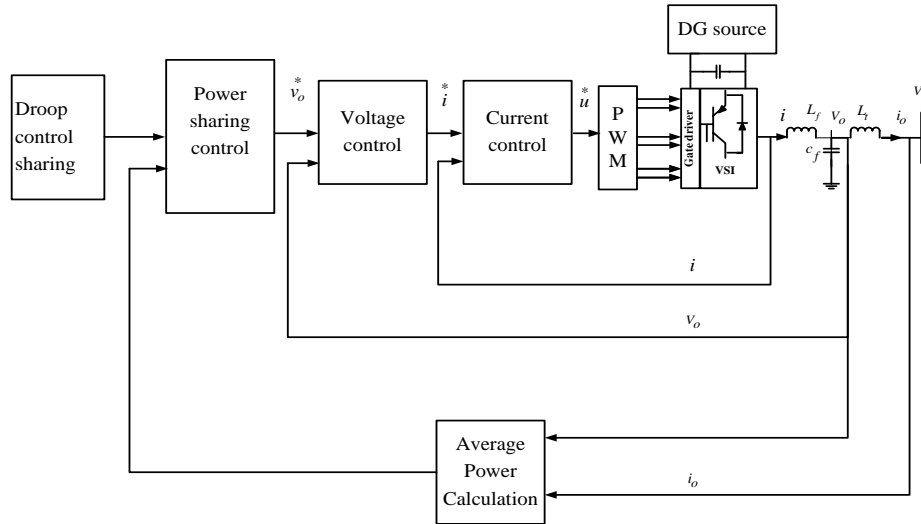

Figure 4. Overall control system structure

The instantaneous active and reactive power components, denoted as p and q, can be accurately determined by employing the two-axis theory.

$$P = (V_{od}I_{od} + V_{oq}I_{oq}) \tag{13}$$

$$Q = (V_{od}I_{oq} + V_{oq}I_{od}) \tag{14}$$

In order to ensure adequate temporal separation between the power and current control loops and to attain optimal power quality injection, the control action involves subjecting the average active and reactive powers associated with the fundamental components to control. These powers are acquired through the utilization of a low pass filter.

$$P = \frac{\omega_c}{s+\omega_c}p \tag{15}$$

$$Q = \frac{\omega_c}{s+\omega_c}q \tag{16}$$

The variable ω_c represents the cut-off frequency of the filter.

The benefits of droop control in a microgrid are its simplicity, high reliability, high flexibility, and the ability to have varying rated powers for each distributed power source [32]. In order to implement a power-sharing function, parallel MC systems commonly employ standard droop characteristics to introduce droops in both the fundamental voltage frequency and magnitude of the output voltage.

$$\omega_o = \omega^* - mP \tag{17}$$

$$v_{od} = V^* - nQ \tag{18}$$

The nominal frequency and voltage set-points are denoted as ω^* and V^*, respectively. The static droop gains, represented by m and n, can be determined for a specific range of frequency and voltage magnitude using (19).

$$m = \frac{\omega_{max} - \omega_{min}}{P_{max}} \tag{19}$$

$$n = \frac{V_{od\,\max} - V_{od\,\min}}{Q_{\max}} \tag{20}$$

The set-points in (17) and (18) act as a virtual communication agent for different MCs and autonomous operation. The d-component of the output voltage is used in (20); as per the voltage-oriented control, the reference of the output voltage magnitude is aligned with the d -axis of the MC reference frame. To provide close voltage regulation, MC output voltage control is adopted. To examine the micro-grid performance with standard controls, the voltage controller employs PI regulators with decoupling and feed-forward control loops to generate the reference current vector. The dynamics of the voltage controller can be given by (21) and (22):

$$i_d^* = k_{pv}(v_{od}^* - v_{od}) + k_{iv}\int(v_{od}^* - v_{od})dt - \omega^* C_f v_{od} + H_{iod} \tag{21}$$

$$i_q^* = k_{pv}(v_{oq}^* - v_{oq}) + k_{iv}\int(v_{oq}^* - v_{oq})dt - \omega^* C_f v_{od} + H_{ioq} \tag{22}$$

The variables k_{pv} and k_{iv} represent the proportional and integral gains, respectively. C_f denotes the filter capacitance, whereas H represents the feed-forward gain. The present controller is required to manipulate the voltage across the filter inductor in order to achieve the lowest possible current error. A traditional PI current regulator with decoupling and feed-forward control loops is utilized to analyze the performance of the micro-grid using conventional controls. The principles governing the current controller can be expressed as (23) and (24):

$$v_d^* = k_{pi}(i_d^* - i_d) + k_{ii}\int(i_d^* - i_d)dt - \omega^* L_f i_q + v_{od} \tag{23}$$

$$v_q^* = k_{pi}(i_q^* - i_q) + k_{ii}\int(i_q^* - i_q)dt - \omega^* L_f i_d + v_{oq} \tag{24}$$

where k_{pv} and k_{ii} are the proportional and integral gains, respectively.

4. SIMULATION RESULTS AND DISCUSSION

To demonstrate the efficacy of the proposed control method in generating the appropriate output voltage and frequency, we simulate and implement the operation of the described matrix converter under various scenarios, including islanding mode. The simulation using the MATLAB/Simulink program has been employed. All simulations assume that the switches of MC are optimal. The input voltages are adjusted by supplying the converters with three-phase voltage transformers that have variable voltage transfer ratios.

4.1. Scenario 1

This research examines three scenarios in order to assess and validate the efficacy of the droop control mechanism, which is based on a proposed switching strategy. Table 2 displays the critical load quantities observed in the 6-bus test MG. In order to demonstrate the efficacy of the suggested droop control, the most severe scenario, referred to as the islanding mode, has been chosen. Figure 2 displays the 6-bus MG, which consists of three sources and five loads. The suggested method is used to analyze the impact of dynamic load changes on the performance of the MG, considering the occurrence of violent changes in loads at different times. Table 3 presents the specified quantities of micro-turbine, diesel generator, and battery.

Table 2. Loads amounts in 6-bus test MG

Load 1	Load 2	Load 3	Load 4	Load 5
P= .38MW	P= .558MW	P= .2MW	P= .3MW	P= .4MW
Q=.25MVar	Q=.22MVar	Q=.2MVar	Q=0MVar	Q=.25MVar

In this case, the occurrence of islanding mode is observed at 1.8 seconds, while a simultaneous load outage is observed at 2.2 seconds in buses 2 and 4, respectively. In this scenario, the energy storage system has been linked to the grid and the circuit breaker for load 2 has been activated. The voltage and frequency profiles for this scenario, as depicted in Figures 5(a) to (h), are presented in the simulation results.

Table 3. The rated amounts of DGs

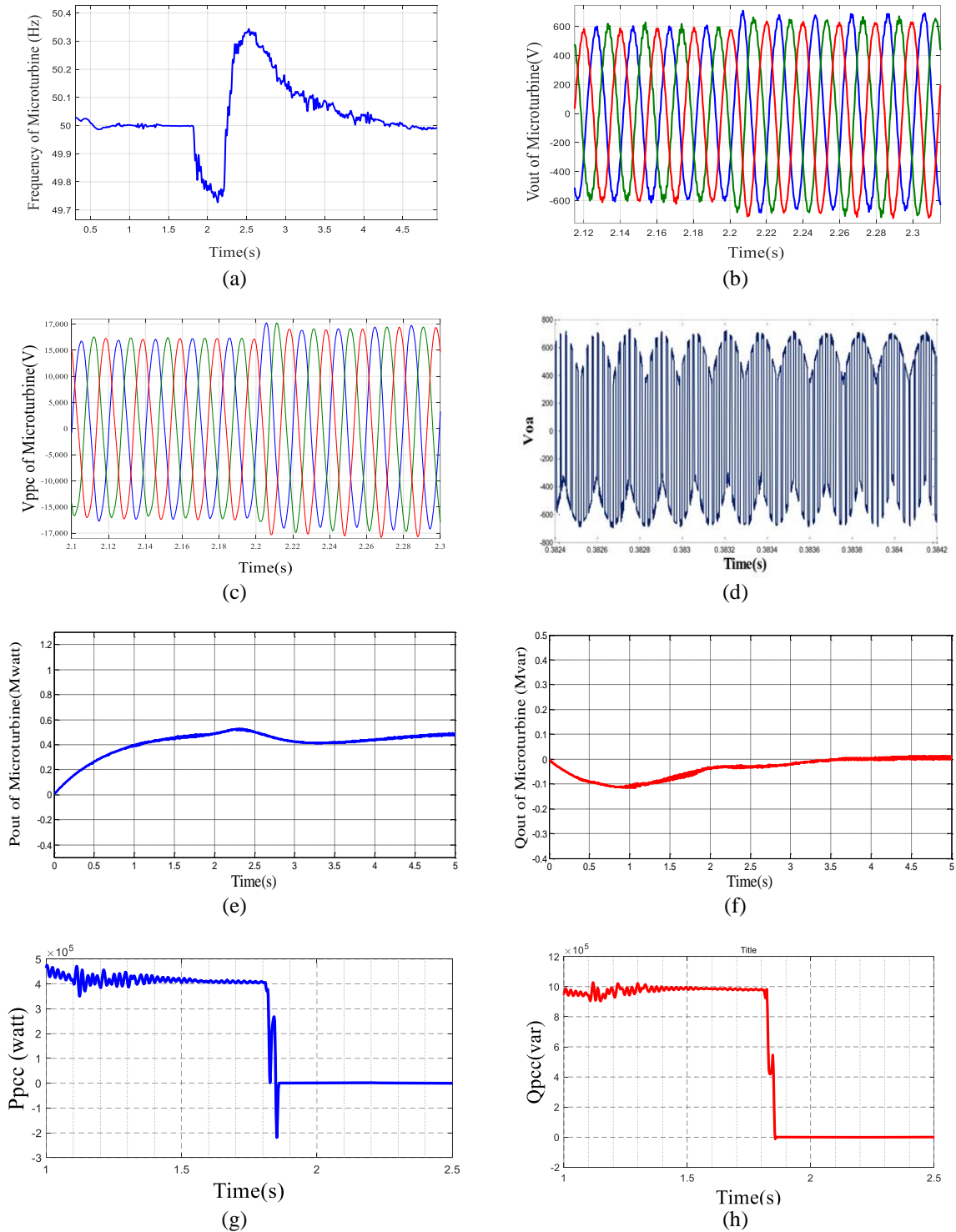| Rated amount	Micro-turbine	Diesel generator	Battery
Voltage and frequency	V=400 V, f=2150 Hz	V=2400 V, f=50 Hz	V=1200
power	S=1 MVA	S=0.5 MVA	S=2.24 MVA

Figure 5. Frequency and voltage profiles in scenario 1 (a) output frequency of micro-turbine,
(b) Output voltages of micro-turbine, (c) PCC voltage of micro-turbine, (d) voltages of micro-turbine before
AC filter, (e) output active power of MG, (f) output reactive power of MG, (g) injected active power of grid,
and (h) injected reactive power of grid

This diagram illustrates the efficacy of the proposed technique in accurately regulating the voltage and frequency of the MG. To restore the steady voltage droop to its nominal operating value, a proportional-integral (PI) controller can be incorporated into the voltage control loop. Furthermore, the output active and reactive power of MG are accurately matched with the reference provided in Figures 5(e) and 5(f), with precise values of 0.4 MW and 0 MVAR, respectively. Figures 5(g) and 5(h) illustrate the active and reactive power at the PCC, which represents the intersection of the grid and microgrid. Figures 5(g) and 5(h) clearly indicate that the injected active power of the system prior to the outage of a large load is 0.4 MW. The total active power of the loads in a microgrid is approximately 1.2 MW. Out of this, 0.4 MW is provided by the grid, while the remaining 0.8 MW, along with line power losses of around 0.45 MW, is supplied by DGs.

4.2. Scenario 2

At time 1.8 sec; islanding mode is occurred and a load is added in bus 3 at time 1.9 sec, respectively. It is noticeable that energy storage has not been connected in grid-connected mode and it connects to MGs at time 2.2 sec by adding another load in bus 4. The voltage and frequency profile of MC in this scenario under this load change are shown in Figure 6. Output frequency of micro-turbine is shown in Figure 6(a) and output voltages of micro-turbine is shown in Figure 6(b). Figure 6(c) illustrates PCC voltage of micro-turbine. It is seen that in t=1.9 sec when a load is added, as shown in Figure 6(a), frequency of MC voltage drops to 49.9 Hz and in worst condition when load and battery are added simultaneously it plunges into lowest amount of 49.6 and then onward reaches to rated frequency. Frequency variations, in this scenario, are stated in the range of 0.8% which is a desirable amount according to standards.
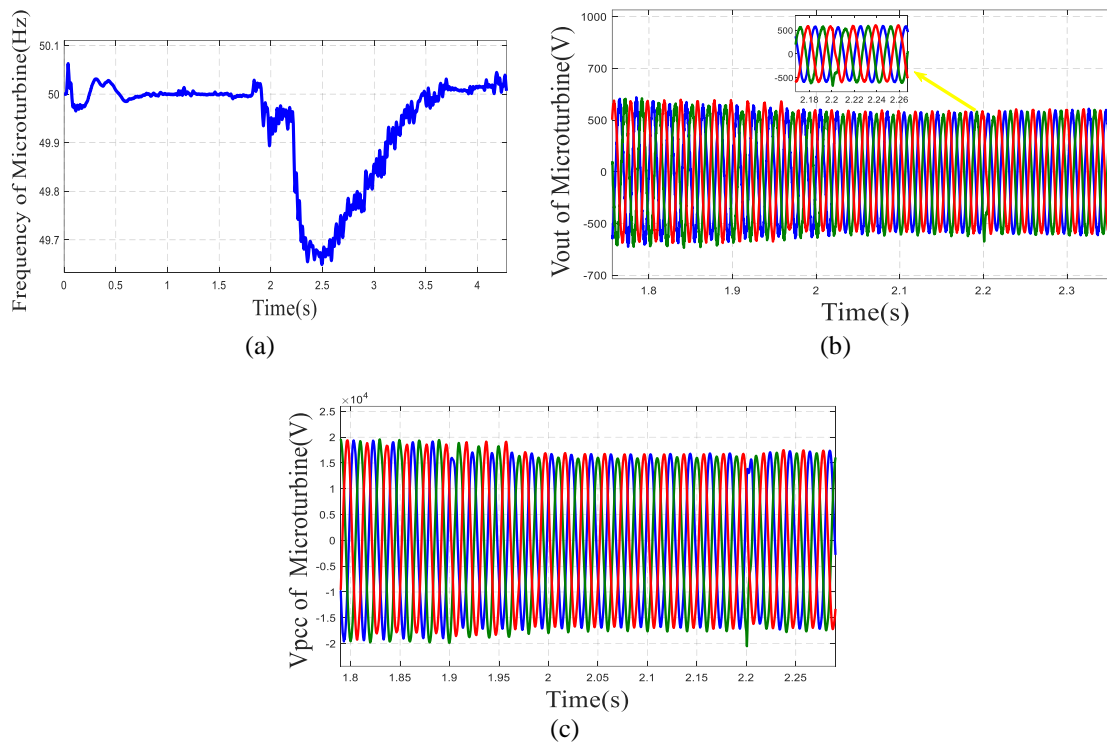

(a)

(b)

(c)

Figure 6. Frequency and voltage profiles in scenario 2 (a) output frequency of micro-turbine,
(b) output voltages of micro-turbine, and (c) PCC voltage of micro-turbine

4.3. Scenario 3

In this scenario, islanding mode occurs at times 1.8 sec and a simultaneous load outage is considered at times 2.2 sec in buses 2 and 4 respectively. In this case, energy storage does not exist in grid-connected mode and connected at time 2.3 sec in islanding mode. The voltage and frequency profile of MC in this scenario under this load change are shown in Figure 7. Figure 7(a) illustrates output frequency of micro-turbine and Figure 7(b) depicts output voltages of micro-turbine. PCC voltage of micro-turbine is shown in Figure 7(c). Figure 8 shows the output powers of MC and battery in this scenario including output active power of MC in Figure 8(a), output reactive power of MC in Figure 8(b), active and reactive powers at output of battery converter in Figure 8(c). As shown in this figure, despite outage of two load simultaneously

in islanding mode without presence of energy storage, they follow desired amounts (maximum amounts) as well as possible. This scenario is selected as an intensive condition between other scenarios, to show capability of suggested method even in controlling of DGs power in our test microgrid.
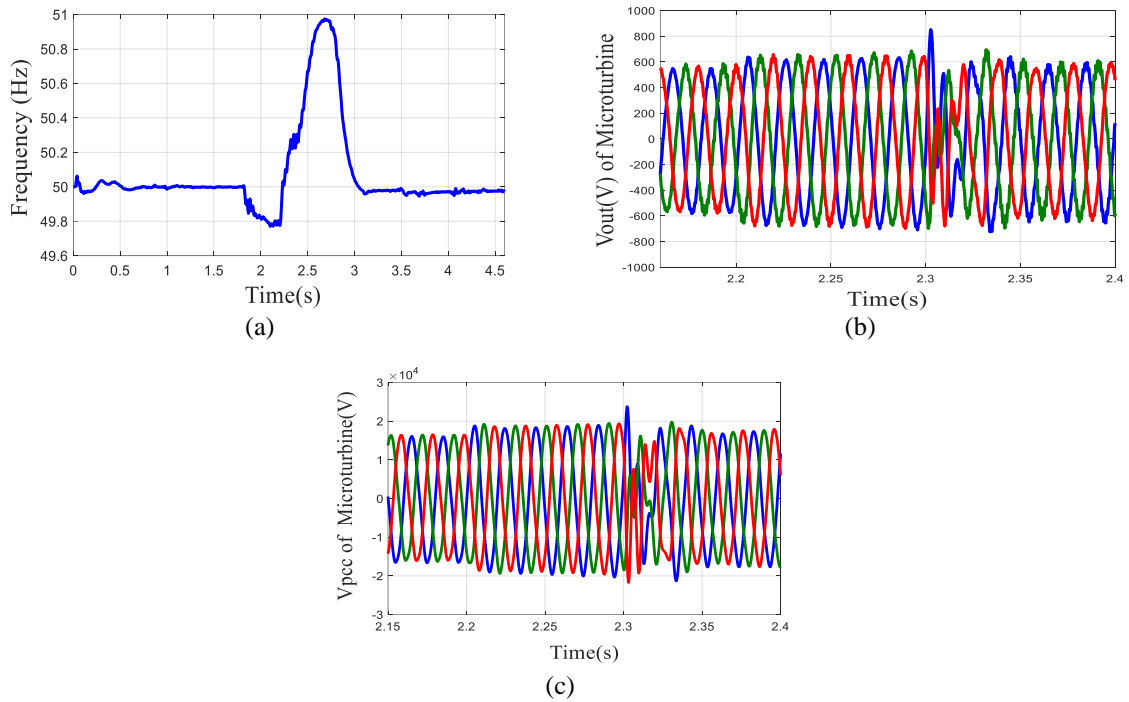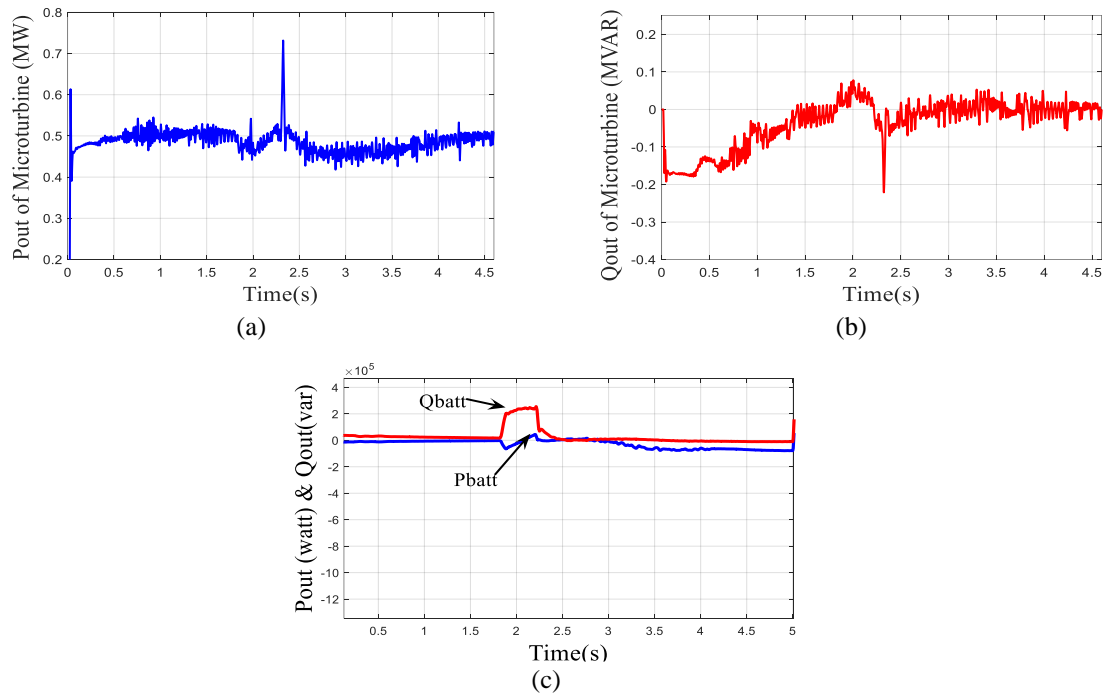

(a)

(b)

(c)

Figure 7. Frequency and voltage profiles in scenario 3. (a) output frequency of micro-turbine, (b) output voltages of micro-turbine, and (c) PCC voltage of micro-turbine

(a)

(b)

(c)

Figure 8. Active and reactive power of micro-turbine in scenario 3 includes exchange of status from grid connected mode to islanding mode. (a) output active power of micro-turbine, (b) output reactive power of micro-turbine, and (c) active and reactive powers at output of battery converter

Reference amounts determined for active and reactive power of micro-turbine are 0.5 MW and 0 MVAR respectively. As shown in Figures 8(a) and 8(b), both active and reactive power follow their references very well. It is noticeable that in this scenario due to load outage, demand load is decreased. Thus, the active power of energy storage is negative and micro-turbine generated active power that charges the battery.

Figure 9 shows the matrix converter input (micro-turbine side) and output (grid side) harmonic spectrums. As shown in Figures 9(a) and 9(b), the amplitude of the fundamental component of the input voltage is 389.6 V that adapts to the line voltage value. THDs of the input and output voltage are 0.84% and 0.15%, respectively. Figure (9) shows that low order harmonics magnitude and THD of input and output voltage of matrix converter with used switching strategy, are low and this approves the high quality of output voltage. Figures 9(c) and 9(d), depict input and output current spectrums which clearly illustrate that low order harmonics magnitude are neglectable. THDs of the input and output current are 1.01% and 4.27%, respectively, which are within the permissible standard range.
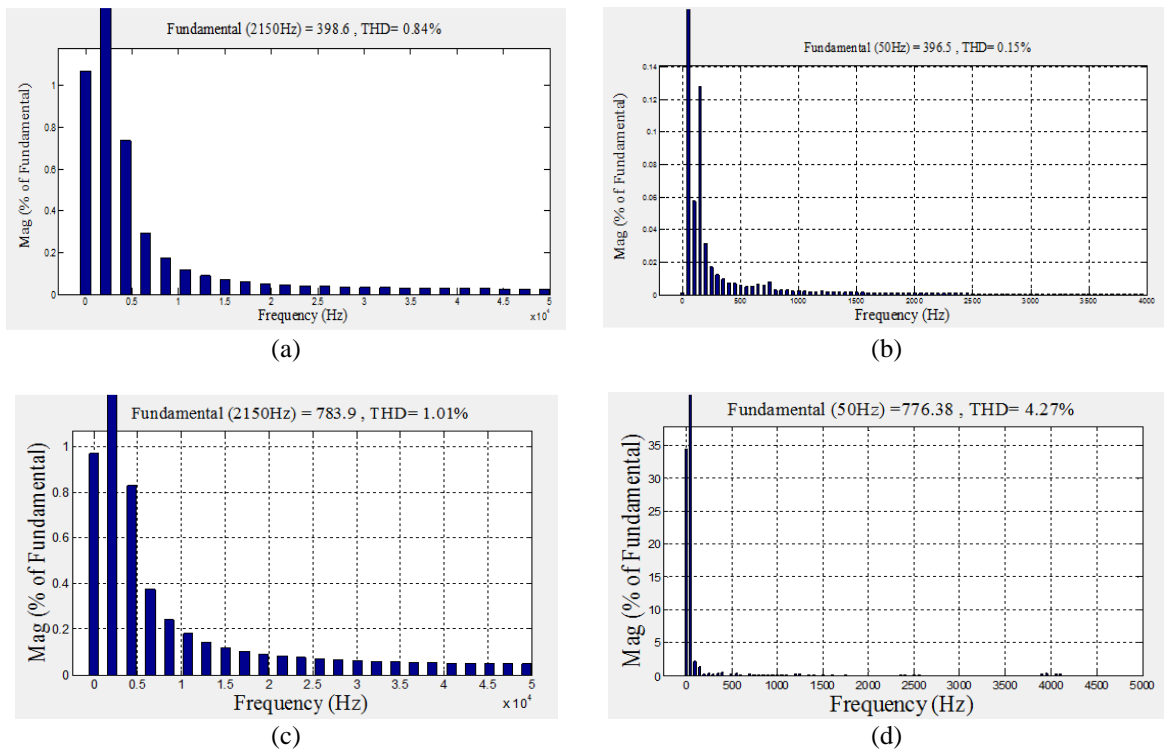

(a)

(b)

(c)

(d)

Figure 9. FFT analysis of input and output voltage in matrix converter interfaced with micro-turbine (a) harmonic spectrum of matrix converter input voltage, (b) harmonic spectrum of matrix converter output voltage, (c) harmonic spectrum of matrix converter input current, and (d) harmonic spectrum of matrix converter output current

Comparing the results associated to this paper with that of [31], it can be seen that voltage and frequency of micro-turbine and other DGs are well controlled after adding or outage of loads in grid-connected or islanding modes. Furthermore, by increasing the number of DGs, the microgrid becomes bulky and hence, the speed of response to islanding mode or load changes will be slower. But, in this paper, by implementing the proposed control method, voltage and frequency of sources have desirable restoration speed in contrast to responses in [31], though there is only one source and load is not changing in [31]. Moreover, the THD value for both output voltage and current of MC interfaced with micro-turbine are considerably lower than the output voltage in [18] with a novel carrier-based Pulse width modulation without narrow pulses for high frequency MC. In this paper, the reference active and reactive power for MC-based micro-turbine and other DGs have been tracked as well and there is no similar former work (microgrid with three power sources and new modulation and control method) with these diverse scenarios and simulation results.

5. CONCLUSION

This study examines the stability of microgrids with a specific focus on the monitoring of micro-turbine voltage and frequency. An alteration in load in a MG system might result in an imbalance between power generation and consumption, hence modifying the output voltage and frequency of the converters. In the event of a sufficiently significant load change, the distributed generators may fail to stabilize the microgrid. The proposed approach involves utilizing PWM to sustain the voltage and frequency of MTG. The proposed methodology has undergone testing on a 6-bus test system across three distinct scenarios. The results demonstrate the stability of MTG or other DGs when there are changes in loads during islanding mode. Furthermore, when employing the recommended approach, the active and reactive capabilities of MTG demonstrate a strong adherence to their respective references. The usefulness of energy storage in stabilizing microgrids, particularly in grid-connected, islanding, and freestanding modes, is widely recognized. The findings demonstrate the strong efficacy of the novel technique, even in the absence of energy storage and standalone MG.

REFERENCES

[1] V. Gurugubelli, A. Ghosh, and A. K. Panda, "Parallel inverter control using different conventional control methods and an improved virtual oscillator control method in a standalone microgrid," *Protection and Control of Modern Power Systems*, vol. 7, no. 1, Dec. 2022, doi: 10.1186/s41601-022-00248-9.

[2] A. Sinha and K. Chandra Jana, "Comprehensive review on control strategies of parallel-interfaced voltage source inverters for distributed power generation system," *IET Renewable Power Generation*, vol. 14, no. 13, pp. 2297–2314, Oct. 2020, doi: 10.1049/iet-rpg.2019.1067.

[3] M. Mirjafari, M. Banejad, H. Molla-Ahmadian, A. Sedehi, and F. Blaabjerg, "Robust stability analysis of a novel droop-based distributed control scheme for islanded operation of DC microgrids," *IET Renewable Power Generation*, vol. 16, no. 15, pp. 3325–3338, Nov. 2022, doi: 10.1049/rpg2.12585.

[4] Y. Li and L. Fan, "Stability analysis of two parallel converters with voltage–current droop control," *IEEE Transactions on Power Delivery*, pp. 1–1, 2017, doi: 10.1109/TPWRD.2017.2656062.

[5] K. Ahmed, I. Hussain, M. Seyedmahmoudian, A. Stojcevski, and S. Mekhilef, "Voltage stability and power sharing control of distributed generation units in DC microgrids," *Energies*, vol. 16, no. 20, Oct. 2023, doi: 10.3390/en16207038.

[6] S. Anderson, P. Hidalgo-Gonzalez, R. Dobbe, and C. J. Tomlin, "Distributed model predictive control for autonomous droop-controlled inverter-based microgrids," in *2019 IEEE 58th Conference on Decision and Control (CDC)*, Dec. 2019, pp. 6242–6248, doi: 10.1109/CDC40024.2019.9028938.

[7] K. R. Patil, S. R. Karnik, and A. B. Raju, "Impacts of distributed generation on power system stability," in *2021 International Conference on Intelligent Technologies (CONIT)*, Jun. 2021, pp. 1–5, doi: 10.1109/CONIT51480.2021.9498452.

[8] A. Abuhaiba, M. Assadi, D. Apostolopoulou, J. Al-Zaili, and A. I. Sayma, "Power transmission and control in microturbines' electronics a review," *Energies*, vol. 16, no. 9, May 2023, doi: 10.3390/en16093901.

[9] H. Hojabri, H. Mokhtari, and L. Chang, "A generalized technique of modeling, analysis, and control of a matrix converter using SVD," *IEEE Transactions on Industrial Electronics*, vol. 58, no. 3, pp. 949–959, Mar. 2011, doi: 10.1109/TIE.2010.2048836.

[10] T. D. Nguyen and H.-H. Lee, "Modulation strategies to reduce common-mode voltage for indirect matrix converters," *IEEE Transactions on Industrial Electronics*, vol. 59, no. 1, pp. 129–140, Jan. 2012, doi: 10.1109/TIE.2011.2141101.

[11] T. D. Nguyen and H.-H. Lee, "A new SVM method for an indirect matrix converter with common-mode voltage reduction," *IEEE Transactions on Industrial Informatics*, vol. 10, no. 1, pp. 61–72, Feb. 2014, doi: 10.1109/TII.2013.2255032.

[12] J. Wang, B. Wu, D. Xu, and N. R. Zargari, "Phase-shifting transformer fed multi-modular matrix converter operated by a new modulation strategy," *IEEE Transactions on Industrial Electronics*, vol. 60, no. 10, pp. 4329–4338, Oct. 2013, doi: 10.1109/TIE.2012.2217714.

[13] S. Li, W. Wang, X. Han, and X. Liu, "A DPWM modulation strategy to reduce common-mode voltage for indirect matrix converters based on active-current vector amplitude characteristics," *IEEE Transactions on Industrial Electronics*, vol. 69, no. 8, pp. 8102–8112, Aug. 2022, doi: 10.1109/TIE.2021.3109503.

[14] J. Rząsa, "Modulation strategy for multi-phase matrix converter with common mode voltage elimination and adjustment of the input displacement angle," *Energies*, vol. 13, no. 3, Feb. 2020, doi: 10.3390/en13030675.

[15] Z. Yan, M. Jia, C. Zhang, and W. Wu, "An integration SPWM strategy for high-frequency link matrix converter with adaptive commutation in one step based on de-re-coupling idea," *IEEE Transactions on Industrial Electronics*, vol. 59, no. 1, pp. 116–128, Jan. 2012, doi: 10.1109/TIE.2011.2158775.

[16] E. Babaei, "A new PWM based control method for forced commutated cycloconverters," *Energy Conversion and Management*, vol. 53, no. 1, pp. 305–313, Jan. 2012, doi: 10.1016/j.enconman.2011.09.012.

[17] F. Blouh, B. Boujidi, and M. Bezza, "Wind energy conversion system based on DFIG using three-phase AC-AC matrix converter," *International Journal of Power Electronics and Drive Systems (IJPEDS)*, vol. 14, no. 3, pp. 1865–1875, Sep. 2023, doi: 10.11591/ijpeds.v14.i3.pp1865-1875.

[18] B. Vasilev and L. Van Tung, "Research methods of V/F control for matrix converter use direct space vector modulation," *International Journal of Electrical and Computer Engineering (IJECE)*, vol. 9, no. 6, pp. 5115–5124, Dec. 2019, doi: 10.11591/ijece.v9i6.pp5115-5124.

[19] X. Wang, T. Wei, R. Wang, Y. Hu, and S. Liu, "A novel carrier-based PWM without narrow pulses applying to high frequency link matrix converter," *IEEE Access*, vol. 8, pp. 157654–157662, 2020, doi: 10.1109/ACCESS.2020.3019086.

[20] S. Toledo *et al.*, "Predictive control applied to matrix converters: a systematic literature review," *Energies*, vol. 15, no. 20, Oct. 2022, doi: 10.3390/en15207801.

[21] Z. Qin, P. C. Loh, and F. Blaabjerg, "Application criteria for nine-switch power conversion systems with improved thermal performance," *IEEE Transactions on Power Electronics*, vol. 30, no. 8, pp. 4608–4620, 2015, doi: 10.1109/TPEL.2014.2360629.

[22] S. Pipolo, A. Formentini, A. Trentin, P. Zanchetta, M. Calvini, and M. Venturini, "A novel matrix converter modulation with reduced number of commutations," *IEEE Transactions on Industry Applications*, vol. 57, no. 5, pp. 4991–5000, Sep. 2021, doi: 10.1109/TIA.2021.3087121.

[23] H. Bevrani and S. Shokoohi, "An intelligent droop control for simultaneous voltage and frequency regulation in islanded microgrids," *IEEE Transactions on Smart Grid*, vol. 4, no. 3, pp. 1505–1513, Sep. 2013, doi: 10.1109/TSG.2013.2258947.

[24] S. Chandak, P. Bhowmik, M. Mishra, and P. K. Rout, "Autonomous microgrid operation subsequent to an anti-islanding scheme," *Sustainable Cities and Society*, vol. 39, pp. 430–448, May 2018, doi: 10.1016/j.scs.2018.03.009.

[25] A. Rashwan, A. Mikhaylov, T. Senjyu, M. Eslami, A. M. Hemeida, and D. S. M. Osheba, "Modified droop control for microgrid power-sharing stability improvement," *Sustainability*, vol. 15, no. 14, Jul. 2023, doi: 10.3390/su151411220.

[26] R. Majumder, A. Ghosh, G. Ledwich, and F. Zare, "Power management and power flow control with back-to-back converters in a utility connected micro grid," *IEEE Transactions on Power Systems*, vol. 25, no. 2, pp. 821–834, May 2010, doi: 10.1109/TPWRS.2009.2034666.

[27] H. Nikkhajoei and R. Iravani, "Steady-state model and power flow analysis of electronically-coupled distributed resource units," *IEEE Transactions on Power Delivery*, vol. 22, no. 1, pp. 721–728, Jan. 2007, doi: 10.1109/TPWRD.2006.881604.

[28] H. R. Baghaee, M. Mirsalim, G. B. Gharehpetian, and H. A. Talebi, "Three-phase AC/DC power-flow for balanced/unbalanced microgrids including wind/solar, droop-controlled and electronically-coupled distributed energy resources using radial basis function neural networks," *IET Power Electronics*, vol. 10, no. 3, pp. 313–328, Mar. 2017, doi: 10.1049/iet-pel.2016.0010.

[29] E. Udoha, S. Das, and M. Abusara, "Power flow management of interconnected AC microgrids using back-to-back converters," *Electronics*, vol. 12, no. 18, Sep. 2023, doi: 10.3390/electronics12183765.

[30] P. Szcześniak, J. Kaniewski, and M. Jarnut, "AC–AC power electronic converters without DC energy storage: a review," *Energy Conversion and Management*, vol. 92, pp. 483–497, Mar. 2015, doi: 10.1016/j.enconman.2014.12.073.

[31] M. Alizadeh and S. S. Kojuri, "Modelling, control, and stability analysis of quasi-Z-source matrix converter as the grid interface of a PMSG-WECS," *IET Generation, Transmission & Distribution*, vol. 11, no. 14, pp. 3576–3585, Sep. 2017, doi: 10.1049/iet-gtd.2017.0178.

[32] H. Lai, K. Xiong, Z. Zhang, and Z. Chen, "Droop control strategy for microgrid inverters: a deep reinforcement learning enhanced approach," *Energy Reports*, vol. 9, pp. 567–575, Sep. 2023, doi: 10.1016/j.egyr.2023.04.263.

BIOGRAPHIES OF AUTHORS

Mahdi Toupchi Khosroshahi holds a M.S. in electrical engineering (power) from Azarbaijan Shahid Madani University, Tabriz, Iran. Currently, he is a collaborative member of the Power Electronic Lab at the Department of Electrical Engineering, Azarbaijan Shahid Madani University. His research interests include renewable energy, micro-grids, smart grids, power electronics, neural network algorithms applications in electric power engineering, power converters, control techniques, optimization with evolutionary algorithms, power system stability, energy storage, artificial intelligence-applied power systems, and FACTS devices. He can be contacted at email: mt.khosroshahy@gmail.com or mt.khosroshahi@azaruniv.ac.ir.

Ali Ajami received his B.Sc. and M.Sc. degrees from the Electrical and Computer Engineering Faculty of Tabriz University, Iran, in electronic engineering and power engineering in 1996 and 1999, respectively, and his Ph.D. degree in 2005 from the Electrical and Computer Engineering Faculty of Tabriz University, Iran, in power engineering. Currently, he is a professor of Electrical Engineering Department of Azarbaijan Shahid Madani University. He is among the top 2% of researchers named by Stanford University and Elsevier BV as the most influential scientists in the world for 2020–present. His main research interests are power electronics converter design, modeling, and controlling; microprocessors; DSP and computer-based control systems; applications of power electronics converters for renewable energy; harmonics and power quality compensation systems; and dynamic and steady-state modeling and analysis of FACTS devices. He can be contacted by email at ajami@azaruniv.ac.ir.

Tole Sutikno is a lecturer and the head of the Master Program of Electrical Engineering at the Faculty of Industrial Technology at Universitas Ahmad Dahlan (UAD) in Yogyakarta, Indonesia. He received his Bachelor of Engineering from Universitas Diponegoro in 1999, Master of Engineering from Universitas Gadjah Mada in 2004, and Doctor of Philosophy in Electrical Engineering from Universiti Teknologi Malaysia in 2016. All three degrees are in electrical engineering. He has been a Professor at UAD in Yogyakarta, Indonesia, since July 2023, following his tenure as an Associate Professor in June 2008. He is the current Editor-in-Chief of TELKOMNIKA and Head of the Embedded Systems and Power Electronics Research Group (ESPERG). He is one of the top 2% of researchers worldwide, according to Stanford University and Elsevier BV's list of the most influential scientists from 2021 to the present. His research interests cover digital design, industrial applications, industrial electronics, industrial informatics, power electronics, motor drives, renewable energy, FPGA applications, embedded systems, artificial intelligence, intelligent control, digital libraries, and information technology. He can be reached via email at tole@te.uad.ac.id.